Supporting Information

Controlled Formation and Binding Selectivity of Discrete Oligo(methyl methacrylate) Stereocomplexes

Jing M. Ren,[†,⊥] Jimmy Lawrence,[†] Abigail S. Knight,[†] Allison Abdilla,[†] Raghida Bou Zerdan,[†] Adam E. Levi,[†] Bernd Oschmann,[†] Will R. Gutekunst,[†] Sang-Ho Lee,[†] Youli Li,[†] Alaina J. McGrath,[†] Christopher M. Bates,[‡,§] Greg G. Qiao,*[,⊥] and Craig J. Hawker*[,†,‡]

[†]Materials Research Laboratory, [‡]Department of Materials, and [§]Department of Chemical Engineering, University of California, Santa Barbara, California 93106, United States, E-mail: hawker@mrl.ucsb.edu

[⊥]Department of Chemical Engineering, The University of Melbourne, Parkville VIC 3010, Australia, E-mail: gregghq@unimelb.edu.au

TABLE OF CONTENTS

GENERAL EXPERIMENTAL SECTION

Materials

Magnesium turnings (Aldrich, > 99.5%), *t*-butylbromide (Alfa Aesar, > 98%), *n*-butyllithium solution (Aldrich, 1.6 M in hexanes), sodium trifluoroacetate (NaTFA, Fluka, ≥ 99.0%), and *trans*-2-[3-(4-*t*-butylphenyl)-2-methyl-2-propenylidene]-malononitrile (DCTB, Fluka, puriss) were used as received. Methyl methacrylate (MMA, TCI, > 99.8%) and 1,1-diphenylethylene (DPE, Alfa Aesar, 98%) were distilled under reduced vacuum over calcium hydride (CaH_2, Sigma-Aldrich, ≥ 97%) before use. Toluene and tetrahydrofuran (THF) were collected under Ar atmosphere from solvent purification system (PureSolv, Innovative Technology Inc.) for polymerization use. Other solvents including acetonitrile (MeCN, Fisher Scientific, 99.5%), diethyl ether (DEE, anhydrous, Sigma-Aldrich, ≥ 99%), toluene (Sigma-Aldrich, 99.5%), ethyl acetate (EtOAc, Sigma-Aldrich, 99.5%), *n*-hexane (Fisher Scientific, 55% as hexane), and anhydrous methanol (Alfa Aesar, 99.9%) were used as received.

Characterization methods

^{1}H and ^{13}C NMR spectroscopy measurements were conducted in $CDCl_3$ at 25 °C or 50 °C on a Varian spectrometer operating at 400 and 100 MHz for ^{1}H and ^{13}C, respectively. For discrete OMMA ($n \leq 10$), the triad tacticity was estimated by integration of the area under the C=O carbon resonance at 175-180 ppm in the ^{13}C NMR spectrum of the crude disperse oligomer. For near-discrete OMMA, the tacticity was estimated by the integration of area under the -CH_3 proton resonance at 0.7-1.3 ppm in the ^{1}H NMR spectrum.[1-2] Small-angle X-ray scattering (SAXS) and wide-angle X-ray scattering (WAXS) measurements were conducted using a custom constructed SAXS/WAXS instrument in the X-ray diffraction facility in the Materials Research Laboratory (MRL) at University of California, Santa Barbara (UCSB). The instrument used a 50 micron microfocus, Cu target X-ray source with a parallel beam multilayer optics and monochromator (Genix from XENOCS SA, France), high efficiency scatterless hybrid slits collimator developed in-house,[3] and Pilatus100k and Eiger 1M solid state detectors (Dectris, Switzerland). The number-average molecular weight (M_n) and weight-average molecular weight (M_w) of the product polymers were determined by GPC in 0.25 wt% triethylamine/chloroform using a Waters 2695 separation module with a Waters 2414 refractive index detector. The columns were calibrated against standard PMMA samples (Agilent Technologies; M_p = 875–1677000 Da; M_w/M_n = 1.02–1.09). Oligo(methyl methacrylate)'s mass spectra were obtained using a Bruker Microflex LRF MALDI TOF mass spectrometer in positive reflectron mode: the analyte, matrix (DCTB) and cationization agent (NaTFA)

were dissolved in THF at concentrations of 10, 10, and 1 mg/mL, respectively, and then mixed in a volume ratio of 10 : 1 : 1. 0.3 μL of this solution was then spotted onto a ground steel target plate, and the solvent was allowed to evaporate prior to analysis. Differential scanning calorimetry (DSC) was performed on a TA Instruments model Q2000 DSC under nitrogen flow. DSC calibration was performed using certified indium and sapphire. To determine the glass transition temperatures (T_g) of the OMMA, the OMMA samples were first heated to 200 ℃ at 10 ℃/min, equilibrated at this temperature for 5 min, and cooled to -50 ℃ at 10 ℃/min. After being held at -50 ℃ for 5 min, the sample was then reheated to 200 ℃ at 10 ℃/min. For determination of the melting temperatures (T_m) and heat of melting (ΔH_m) of OMMA stereocomplexes, samples were heated to 200 ℃ at 10 ℃/min, and cooled down to 40 ℃ at 10 ℃/min before the next measurement. OMMA stereocomplex samples were dried under vacuum (0.05 mmHg) for 12 h prior to DSC analysis.

Oligomerization procedures

Isotactic oligo(methyl methacrylate) (it-OMMA) synthesis

it-OMMA was synthesized by anionic polymerization with adapted published procedures.[4-5] The Grignard reagent, *t*-C_4H_9MgBr, was prepared as follows: anhydrous DEE (28 mL) and *t*-butylbromide (14 g, 0.10 mol) were added consecutively into a dry addition funnel under N_2. Separately, Mg turnings (3.7 g, 0.15 mol) were added to a dry round bottom flask under N_2 via a funnel with a flushing adapter, followed by the addition of anhydrous DEE (60 mL). The *t*-butylbromide solution was then added slowly at 25 °C over 1 h. The solution was stirred for a further hour and then left to stand for 12 hours. The Grignard reagent ($[t\text{-}C_4H_9MgBr]_{eff}$ = 360 mM determined via polymerization) was stored in a dry round-bottom flask equipped with a 3-way stopcock under Ar atmosphere at 0 °C before use.

The general procedure employed for the synthesis of *it*-OMMA: the Grignard reagent (10 mL, 1 equiv.) was added to anhydrous toluene (57 mL) in a Schlenk tube at -78 °C under Ar. MMA was then added dropwise (4.6 mL in 5 min, 12 quiv.) causing the mixture to turn orange. The polymerization solution was kept at -78 °C for 30 h, and then degassed anhydrous methanol (5 mL) was added to the Schlenk flask to quench the reaction. The reaction solution was diluted with toluene (50 mL), washed with 2 M HCl (50 mL × 3) and distilled water (50 mL × 3), dried ($MgSO_4$), filtered and concentrated to obtain *it*-OMMA as a waxy solid, 3.50 g (83 %); ^{13}C NMR: *mm*/*mr*/*rr* (%) = 80/10/10. GPC data, ^1H and ^{13}C NMR, and FT-IR spectra are provided in **Figure S17a-d**. The same synthesis was repeated to yield more low MW materials and the high MW crude *it*-OMMA (by changing the monomer-to-initiator ratio) for subsequent chromatography purification.

Syndiotactic oligo(methyl methacrylate) (st-OMMA) synthesis

The general procedure for *st*-OMMA synthesis via anionic polymerization was adapted from previous literature and is described as follows:[6] the initiator 1,1-diphenyl-*n*-hexyllithium (*n*-Hex(Ph)$_2$Li) was prepared in-situ by adding DPE (0.55 mL, 1 equiv.), and *n*-butyllithium (1.6 M in hexane, 2 mL, 1 equiv.) to anhydrous THF (48 mL) in a Schlenk tube at room temperature under Ar. The initiator solution was stirred for 2 h before cooling down to -78 °C in a MeOH/dry ice bath. MMA was then added dropwise (5 mL in 5 min, 15 equiv.) to start the oligomerization. The reaction solution was kept at -78 °C for 1 h, and then degassed anhydrous methanol (5 mL) was added to the Schlenk flask to quench the reaction. The oligomerization solution was diluted with toluene (50 mL), passed through a silica gel plug and concentrated to obtain *st*-OMMA as a white powder, 5.0 g (95 %); ^{13}C NMR: *mm*/*mr*/*rr* (%) = 1/24/75. GPC data and ^{1}H and ^{13}C NMR spectra are provided in **Figure S17e-g**. The same synthesis was repeated to yield more low MW materials and the high MW crude *st*-OMMA (by changing the monomer-to-initiator ratio) for subsequent chromatography purification.

Isolation of near-discrete oligo(methyl methacrylate)

Automatic flash chromatography separation of oligo(methyl methacrylate) was performed on a Biotage Isolera One unit coupled with a Biotage ESLD-A120 detector using Biotage KP-SIL SNAP/SNAP Ultra cartridge series (100 g/340 g for 2/10 g separation), eluting with MeCN/Toluene using the gradient profile according to our previous publication:[7]

% MeCN (Start)	% MeCN (End)	Column Volume (CV)
0	25	15
25	50	15

Representative characterization data (MALDI-ToF, GPC, DSC, and XRD) of separated *it*-OMMA and *st*-OMMA can be found in **SI 1-9**. Representative ^{1}H NMR spectra (for tacticity determination) and FT-IR of the isolated OMMA (using *it*-/*st*-20 as illustrative examples) can be found in **Figure S17h - j**.

Preparation of OMMA stereocomplexes in dilute solution

The general procedure employed for the synthesis of OMMA stereocomplexes was as follows:[8] *st*-OMMA (10 mg) and *it*-OMMA (10 mg) precursors were separately dissolved in MeCN:H_2O (9:1) at concentrations of 2 mg/mL and combined to an *it*:*st* molar ratio of 1:2. The solutions were left to stand at room temperature for 24 h. After removing the solvent *in vacuo*, the stereocomplexes were dried under reduced pressure (0.05 mmHg)

for 24 h before DSC and XRD analysis. Representative examples of the DSC and XRD curves of the OMMA stereocomplexes are shown in **Figure S6**.

For the competitive binding experiments, the *it*-/*st*-components were combined to an *it*:*st* molar ratio of 1:1 or 1:4 (either *it*- or *st*- in excess). The solutions were left to stand at room temperature for 24 h. The stereocomplex precipitates were then collected via centrifugation, and dried under reduced pressure (0.05 mmHg) for 24 h before GPC and MALDI-MS (for *st*-25/40 and *it*-80 experiment only) analysis. The GPC and MALDI-MS data for the competitive binding experiments were provided in **Figure S14-16**.

CHARACTERIZATION DATA

SI-1. Characterization of low DP *it*-OMMA separation

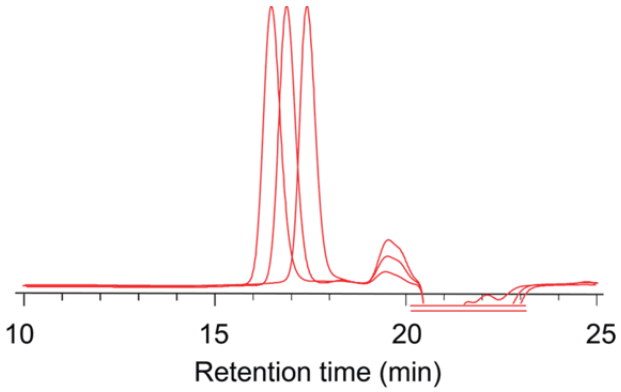

Figure S1. GPC traces of isolated *it*-5, 10, and 15.

Table S1. Result summary of low DP *it*-OMMA separation

Sample	MALDI-ToF MS		GPC		NMR	Tacticity	T_g
	M_n	$Đ$	M_n	$Đ$	M_n	*mm/mr/rr*	(°C)
***it*-5**	559	1.000	600	1.06	560	80/10/10	7
***it*-10**	1100	1.001	1200	1.06	1100	80/10/10	11
***it*-15**	1600	1.002	1800	1.06	1500	91/7/2	21

***SI*-2. MALDI-ToF MS spectra of the isolated low DP *it*-OMMA and *st*-OMMA**

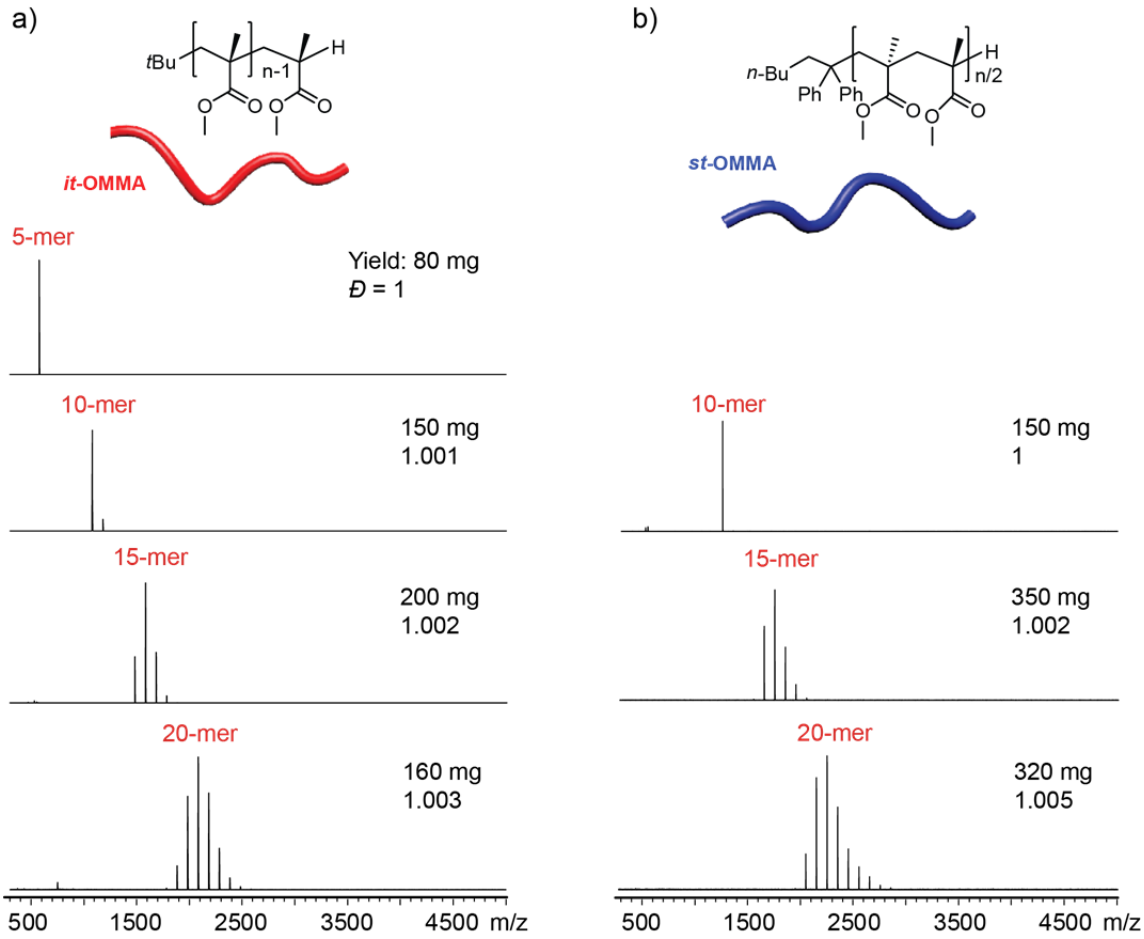

Figure S2. MALDI-ToF MS of representative (near-)discrete (a) *it*-OMMA and (b) *st*-OMMA isolated from 10 g-scale separations.

SI-3. Characterization data comparison of the crude and isolated OMMA

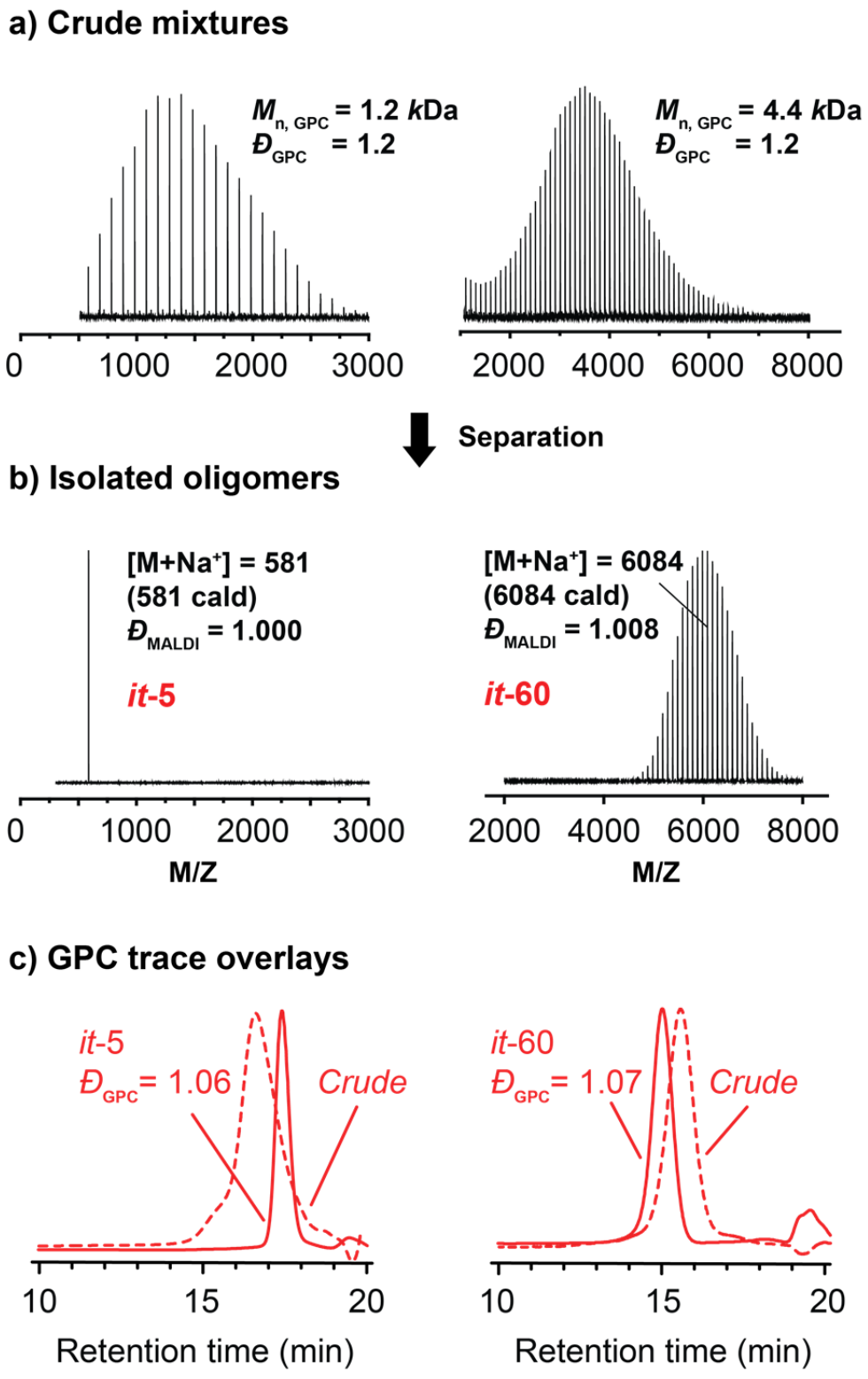

Figure S3. MALDI-ToF mass spectra of the a) crude and b) isolated *it*-OMMAs (DP = 5 and 60) and c) GPC trace overlays of the crude and isolated OMMAs.

SI-4. DSC and XRD traces of disperse it-DP11/st-DP15 stereocomplex

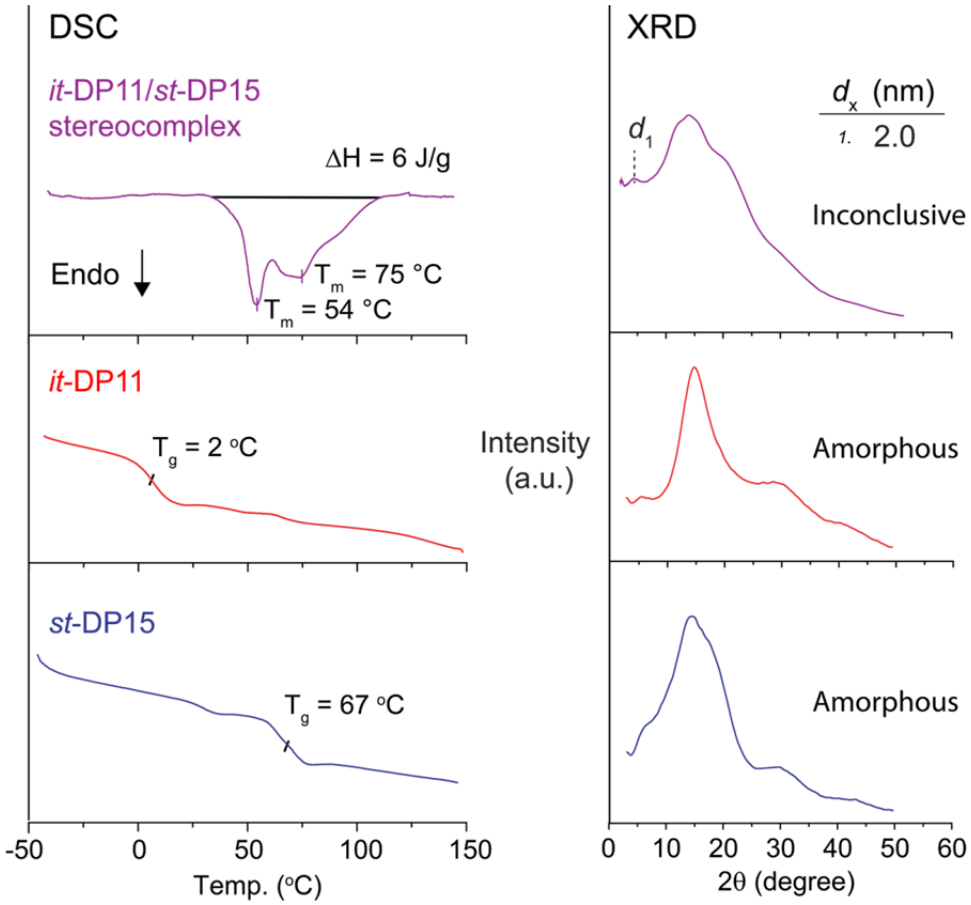

Figure S4. DSC and XRD traces of disperse *it*-DP11/*st*-DP15 stereocomplex (*it*-/*st*- molar ratio = 1:2), and the OMMA precursors (i.e., *it*-DP11 and *st*-DP15).

***SI*-5. ^{13}C NMR spectrum of the crude *it*-OMMA oligomeric mixture**

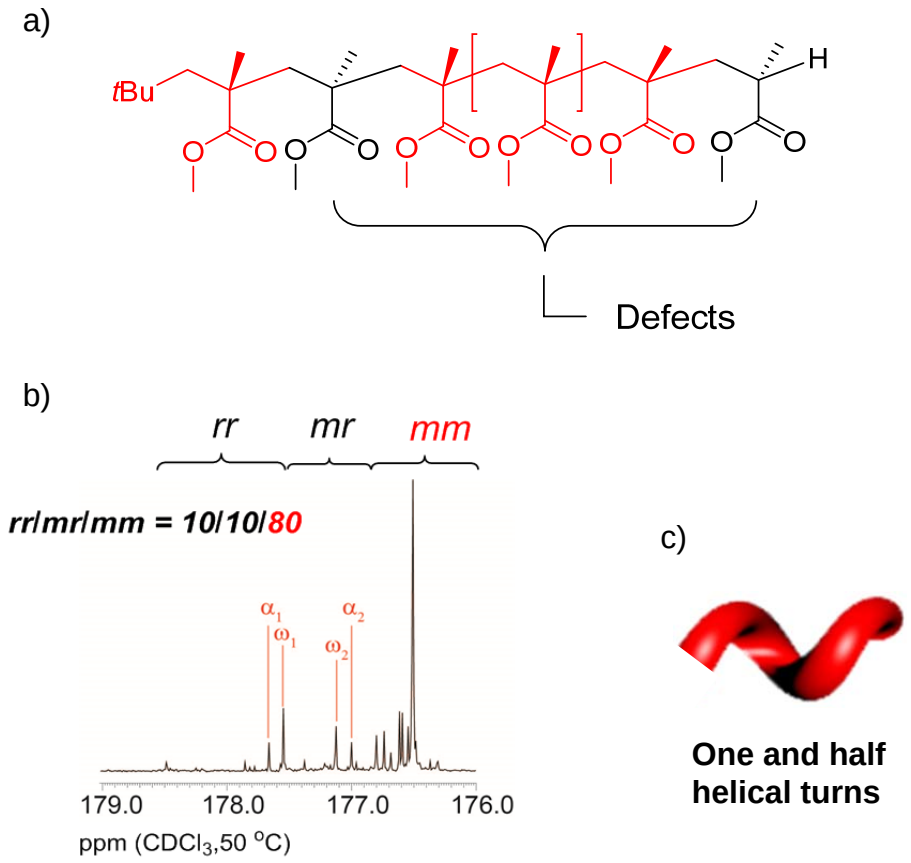

Figure S5. (a) An example of a chemical structure for the crude *it*-OMMA prepared from living anionic oligomerization showing the potential sequence defects. (b) ^{13}C NMR spectra of the *it*-OMMA showing imperfection in stereoregularity (*mm* = 80%). (c) The helical model of *it*-OMMA at the critical chain length.

***SI*-6. Diad tacticity and relative abundance calculations for isolated OMMA**

Table S2. Additional tacticity characterization of OMMA

Sample	*Triad Tacticity*			*Diad Tacticity*		*Abundance (%)**
isotactic (it-)	***mm***	***mr***	***rr***	***m***	***r***	**(P*m* or P*r*)$^{n-1}$**
***it*-5**	80	10	10	85	15	52
***it*-10**	80	10	10	85	15	23
***it*-15**	91	7	2	95	5	45
***it*-20**	90	8	2	94	6	31
***it*-30**	92	5	3	95	5	19
***it*-40**	88	7	5	92	8	3
***it*-60**	89	6	5	92	8	1
syndiotactic (st-)						
***st*-10**	1	24	75	13	87	29
***st*-15**	13	12	75	19	81	5
***st*-20**	10	13	77	17	83	3
***st*-30**	8	14	78	15	85	1
***st*-40**	7	14	79	14	86	0
***st*-60**	4	15	81	11	89	0

***** Percentage of perfect tacticity chains (e.g., DP = 5, P*m* = 0.85 and abundance $(0.85)^4 \times 100\% = 52\%$)

***SI*-7. DSC and XRD traces of near-discrete and disperse DP20 OMMA stereocomplexes**

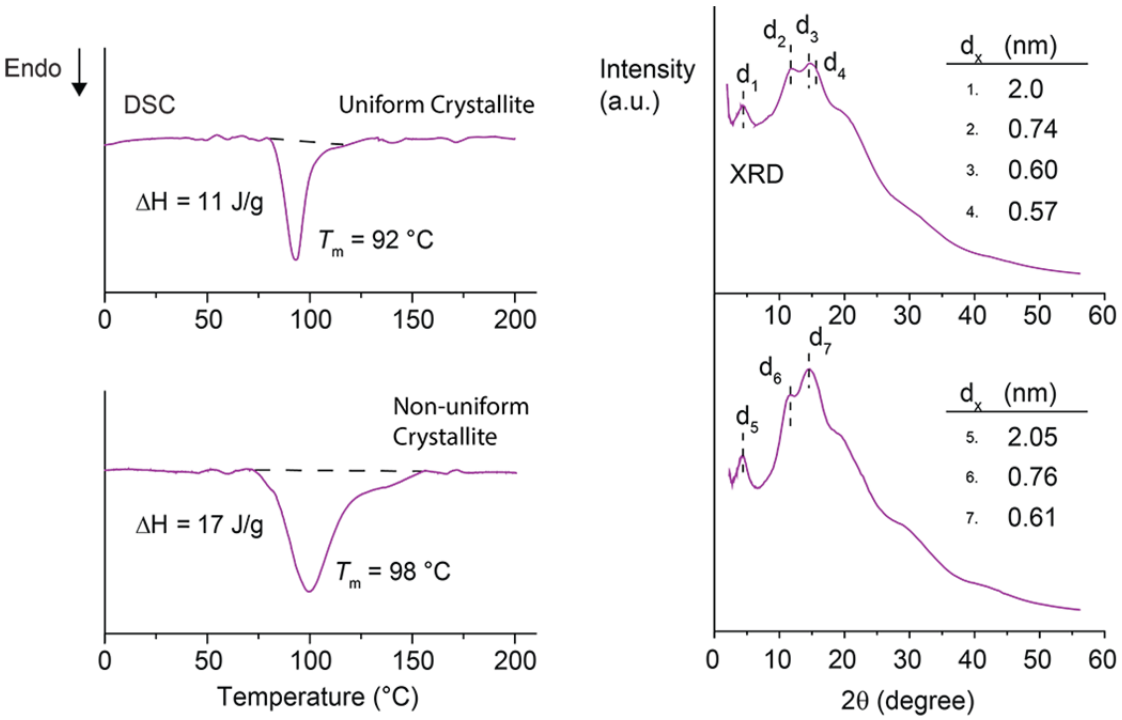

Figure S6. DSC and XRD traces of near-discrete (i.e., *it*-20/*st*-20) stereocomplex (top), and disperse (i.e., *it*-DP20/*st*-DP20) stereocomplex (bottom) (*it*-/*st*- molar ratio = 1:2).

***SI*-8. Characterization of high DP *it*-OMMA separation**

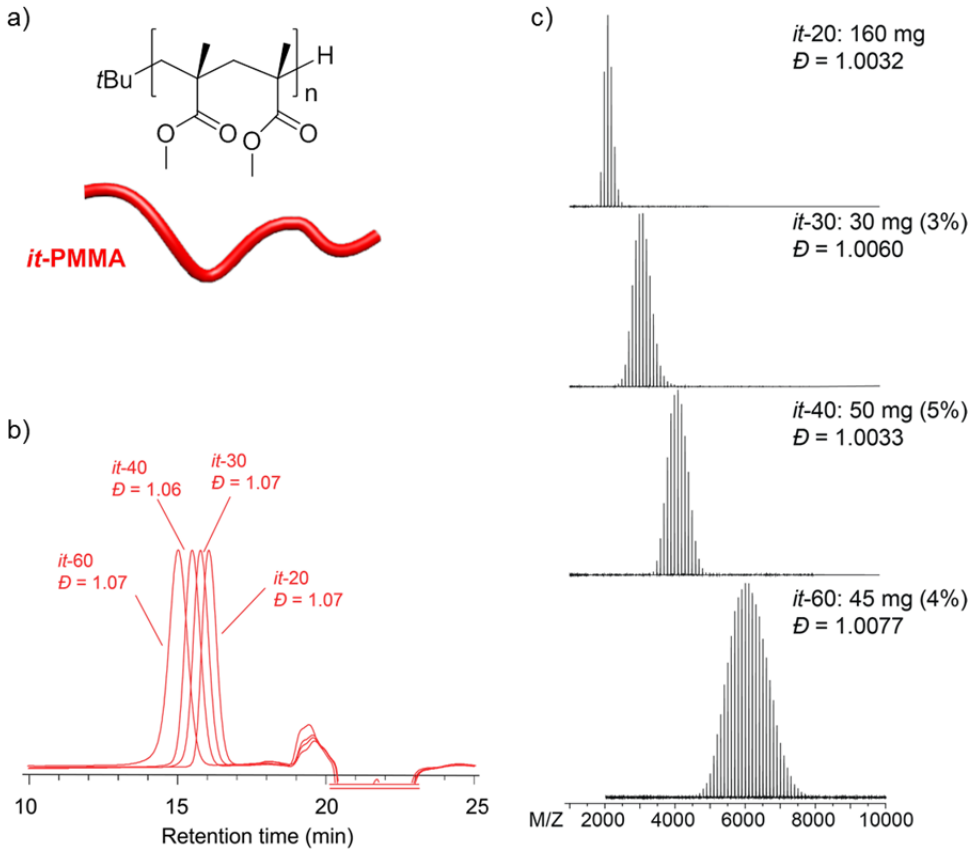

Figure S7. (a) Chemical structure of *it*-OMMA (b) GPC traces of isolated *it*-20, 30, 40, and 60 OMMA samples. (c) MALDI-ToF MS of isolated near-discrete *it*-20, 30, 40, and 60 OMMA samples.

Table S3. Result summary of high DP *it*-OMMA separation

	MALDI-ToF MS		GPC		NMR	Tacticity	T_g
Sample	M_n	Đ	M_n	Đ	M_n	*mm/mr/rr*	(°C)
***it*-20**	2100	1.003	2500	1.07	2200	90/8/2	26
***it*-30**	3000	1.006	3700	1.07	2800	92/5/3	37
***it*-40**	4000	1.003	4900	1.06	3700	88/7/5	40
***it*-60**	6100	1.008	7900	1.07	6000	89/6/5	42

SI-9. Characterization of high DP *st*-OMMA separation

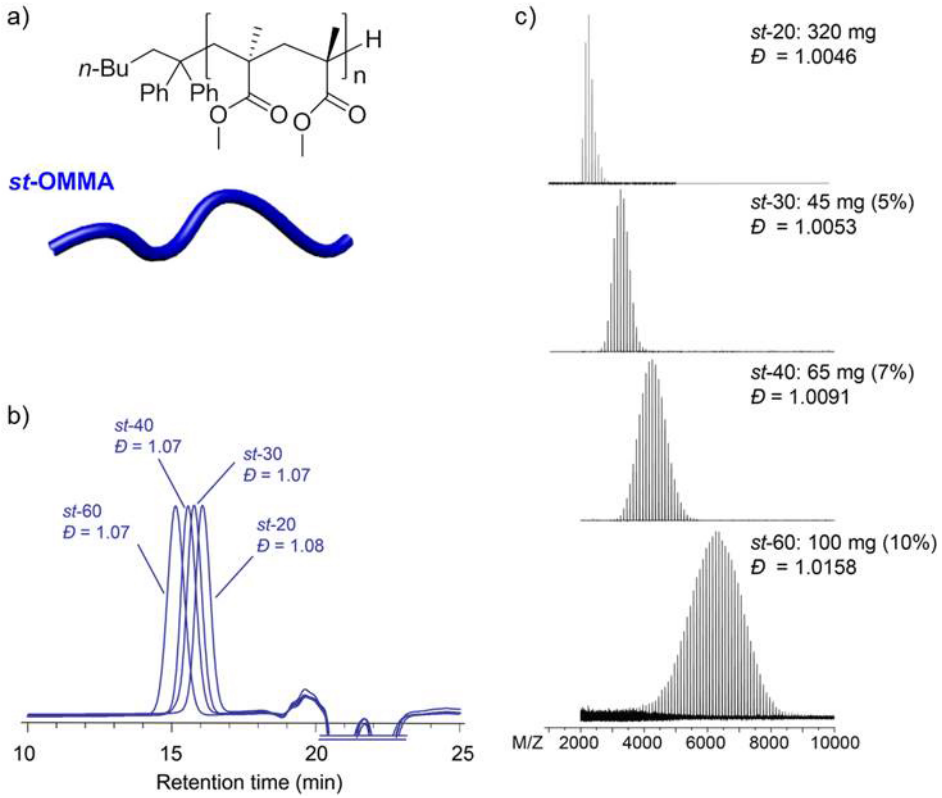

Figure S8. (a) Chemical structure of *st*-OMMA (b) GPC traces of isolated *st*-20, 30, 40, and 60 OMMA samples. (c) MALDI-ToF MS of isolated near-discrete *st*-20, 30, 40, and 60 OMMA samples.

Table S4. Result summary of high DP *st*-OMMA separation

	MALDI-ToF MS		GPC		NMR	Tacticity	T_g
Sample	M_n	Đ	M_n	Đ	M_n	*mm/mr/rr*	(°C)
***st*-20**	2300	1.005	2700	1.08	2600	10/13/77	83
***st*-30**	3300	1.005	3800	1.07	3400	8/14/78	86
***st*-40**	4300	1.009	4700	1.07	4500	7/14/79	94
***st*-60**	6400	1.016	7100	1.07	6000	4/15/81	101

***SI*-10. MW effects of *it*-OMMA on the stereocomplex melting temperatures**

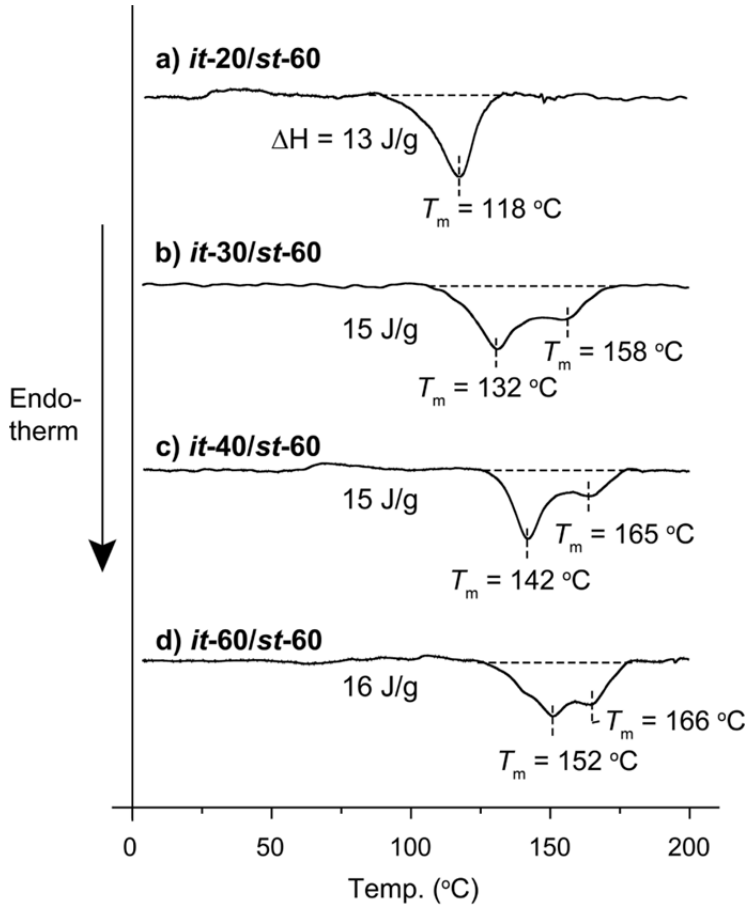

Figure S9a. DSC traces of OMMA stereocomplexes prepared from a) *it*-20/*st*-60, b) *it*-30/*st*-60, c) *it*-40/*st*-60, and d) *it*-60/*st*-60 pairs, respectively (*it*-/*st*- molar ratio = 1:2).

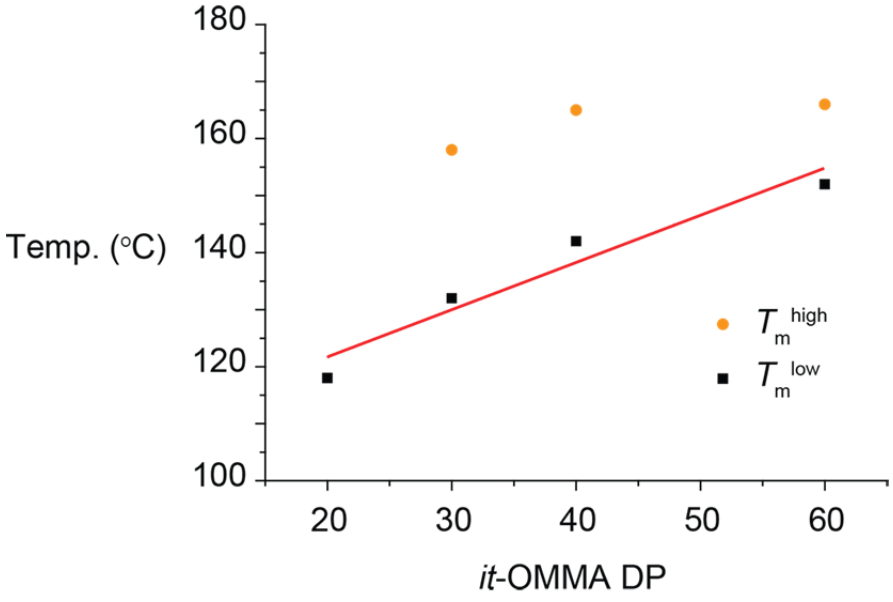

Figure S9b. Linear plot shows that DP increase in the *it*-OMMA precursor will increase the melting temperature of the OMMA stereocomplexes (*it*-/*st*- molar ratio = 1:2).

***SI*-11. MW effects of *st*-OMMA on the stereocomplex melting temperatures**

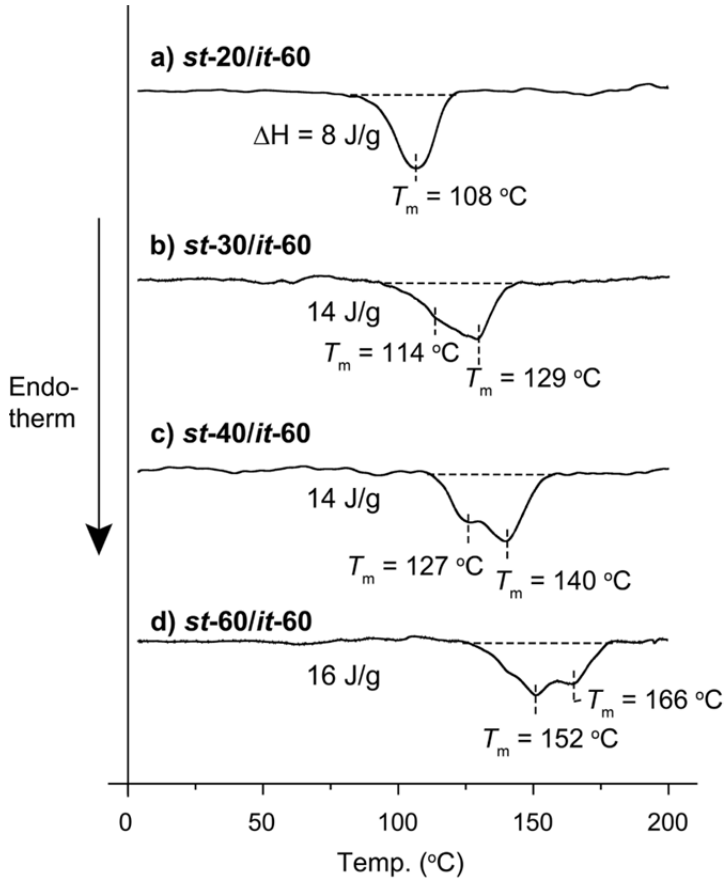

Figure S10a. DSC traces of OMMA stereocomplexes prepared from a) *st*-20/*it*-60, b) *st*-30/*it*-60, c) *st*-40/*it*-60, and d) *st*-60/*it*-60 pairs, respectively (*it*-/*st*- molar ratio = 1:2).

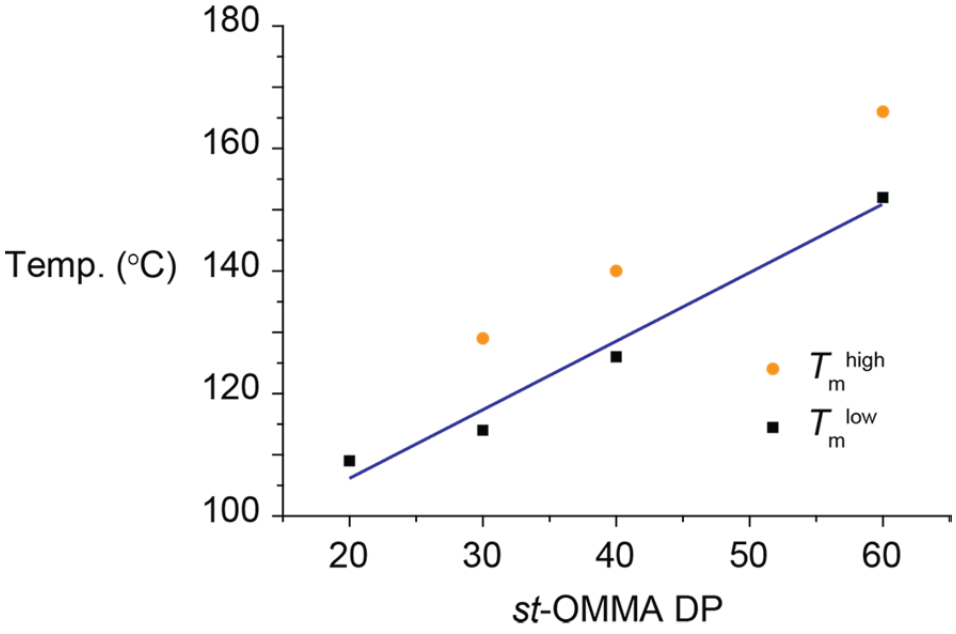

Figure S10b. Linear plot shows that DP increase in the *st*-OMMA precursor will increase the melting temperature of the OMMA stereocomplexes (*it*-/*st*- molar ratio = 1:2).

***SI*-12. DSC and Variable Temperature (VT) XRD profiles illustrating disassembly of the OMMA triple-helices during the melting of the stereocomplexes**

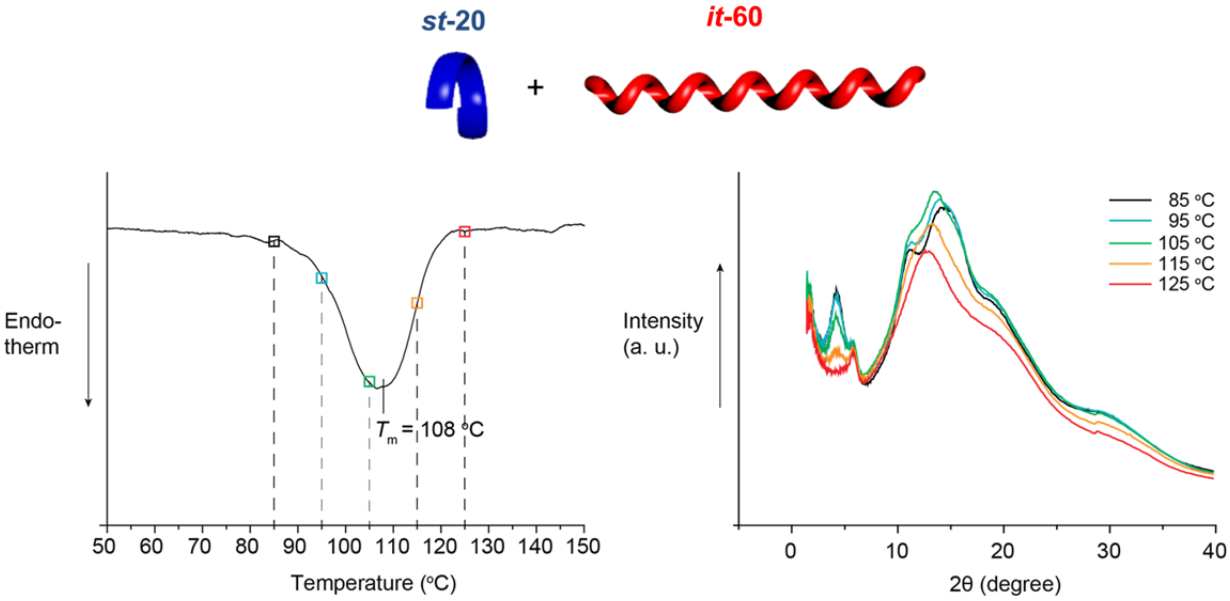

Figure S11a, DSC curve and XRD profiles of the *st*-20/*it*-60 stereocomplex (*it*-/*st*- molar ratio = 1:2) at different temperatures across the endothermic peak.

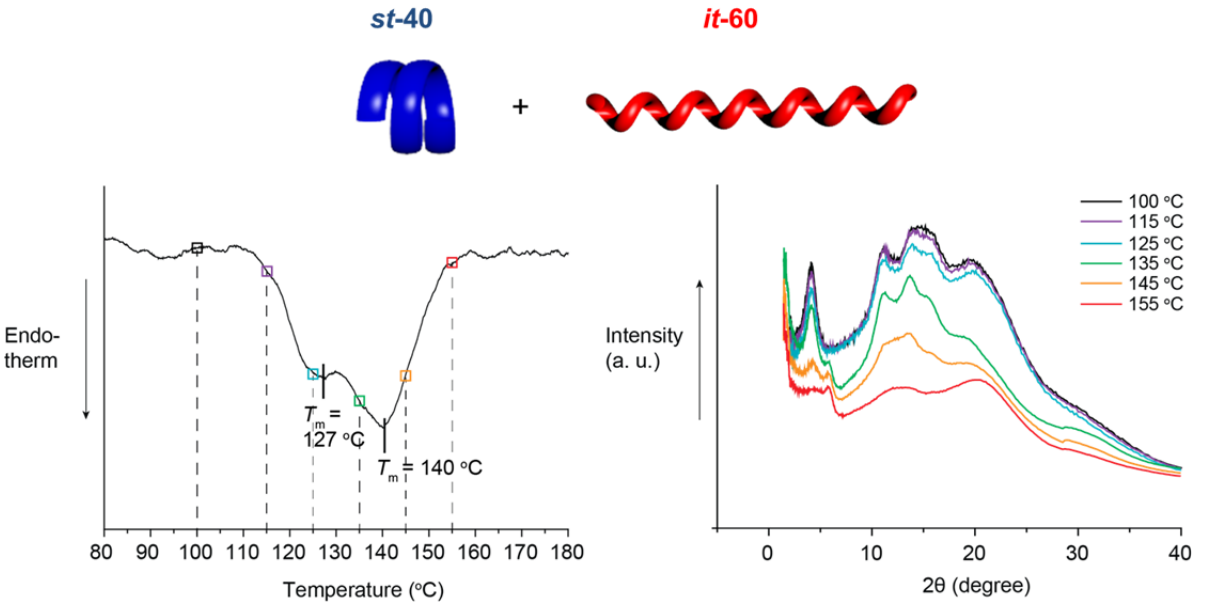

Figure S11b, DSC curve and XRD profiles of the *st*-40/*it*-60 stereocomplex (*it*-/*st*- molar ratio = 1:2) at different temperatures across the endothermic peaks.

***SI*-13. Diagrams illustrate the crystallization mechanism of the OMMA stereocomplex**

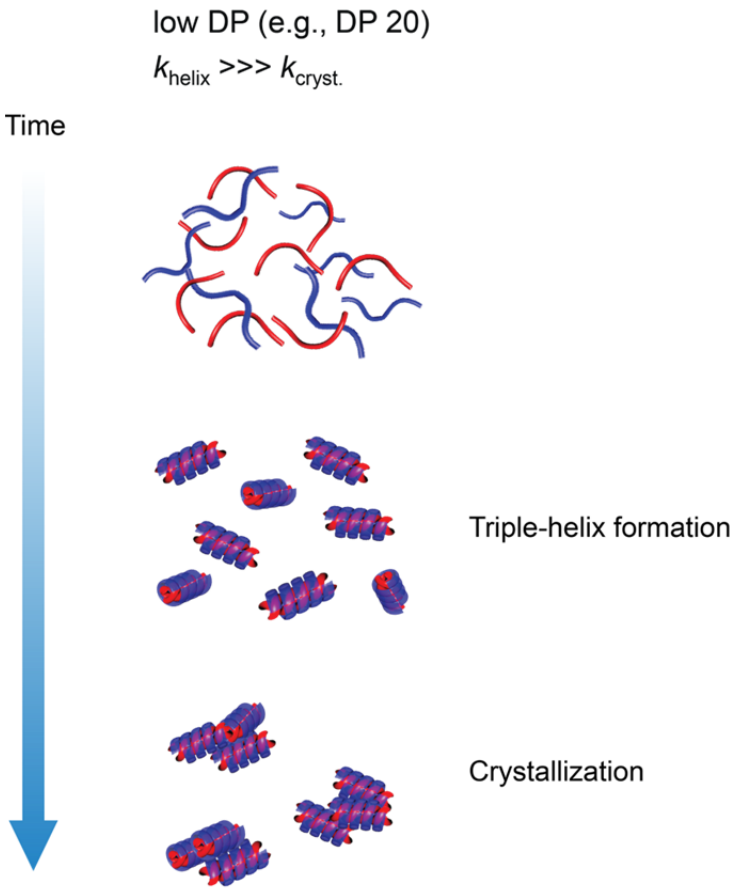

Figure S12a. Schematic illustration of the crystallization of low MW stereoregular OMMAs via the 'micellar' growth, adapted from the previous work by Schomaker and Challa.[9]

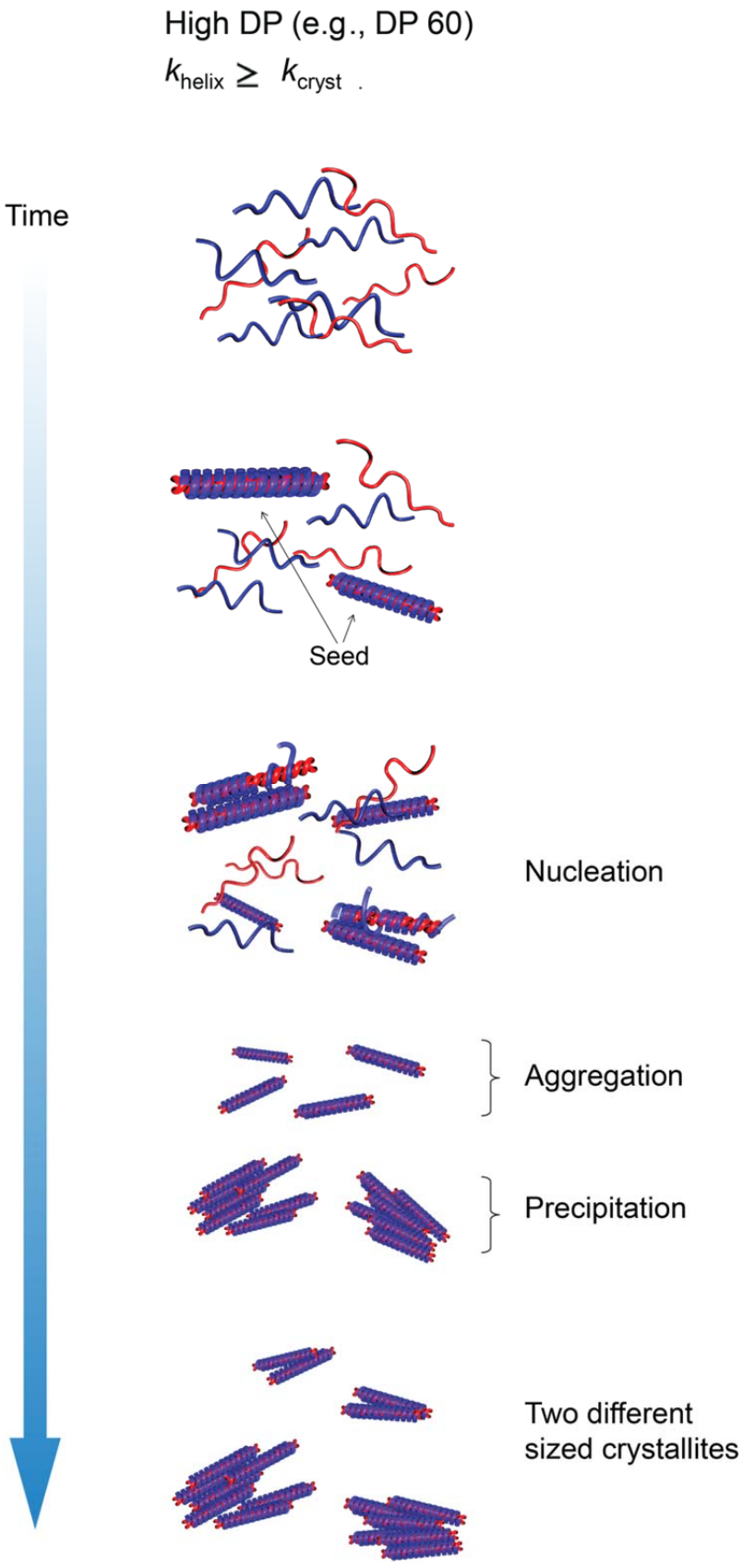

Figure S12b. Schematic illustration of the crystallization of high MW stereoregular OMMAs via both the 'fringed-micellar' and 'lamellar' growths, adapted from the previous work by Schomaker and Challa.[9]

SI-14. **Tailoring melting behavior of the stereocomplex by customizing the MWD of OMMA**

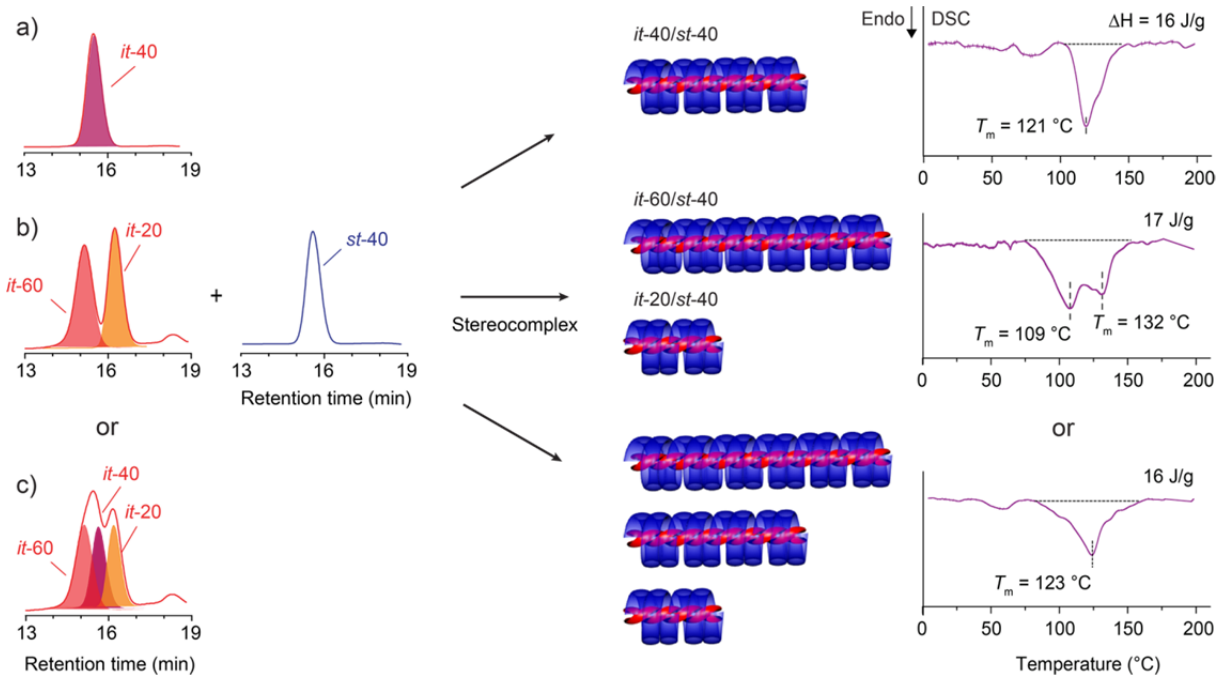

Figure S13. GPC and DSC results demonstrate it is possible to tailor the endothermic transition of the stereocomplex materials (from a single sharp peak, to two peaks to a broad peak) by customizing the MWD of the stereoregular oligomer component. *it*-OMMA artificial blends consist of a) single component: *it*-40, b) dual component *it*-20 and *it*-60, and c) tri-component: *it*-20, *it*-40, and *it*-60. (i.e., with a mono-, bi- and trimodal MWD, respectively) (*it*-/*st*- molar ratio = 1:2).

***SI-15*. Molecular separation of *st*-25 and 40 through stereocomplex formation with *it*-80**

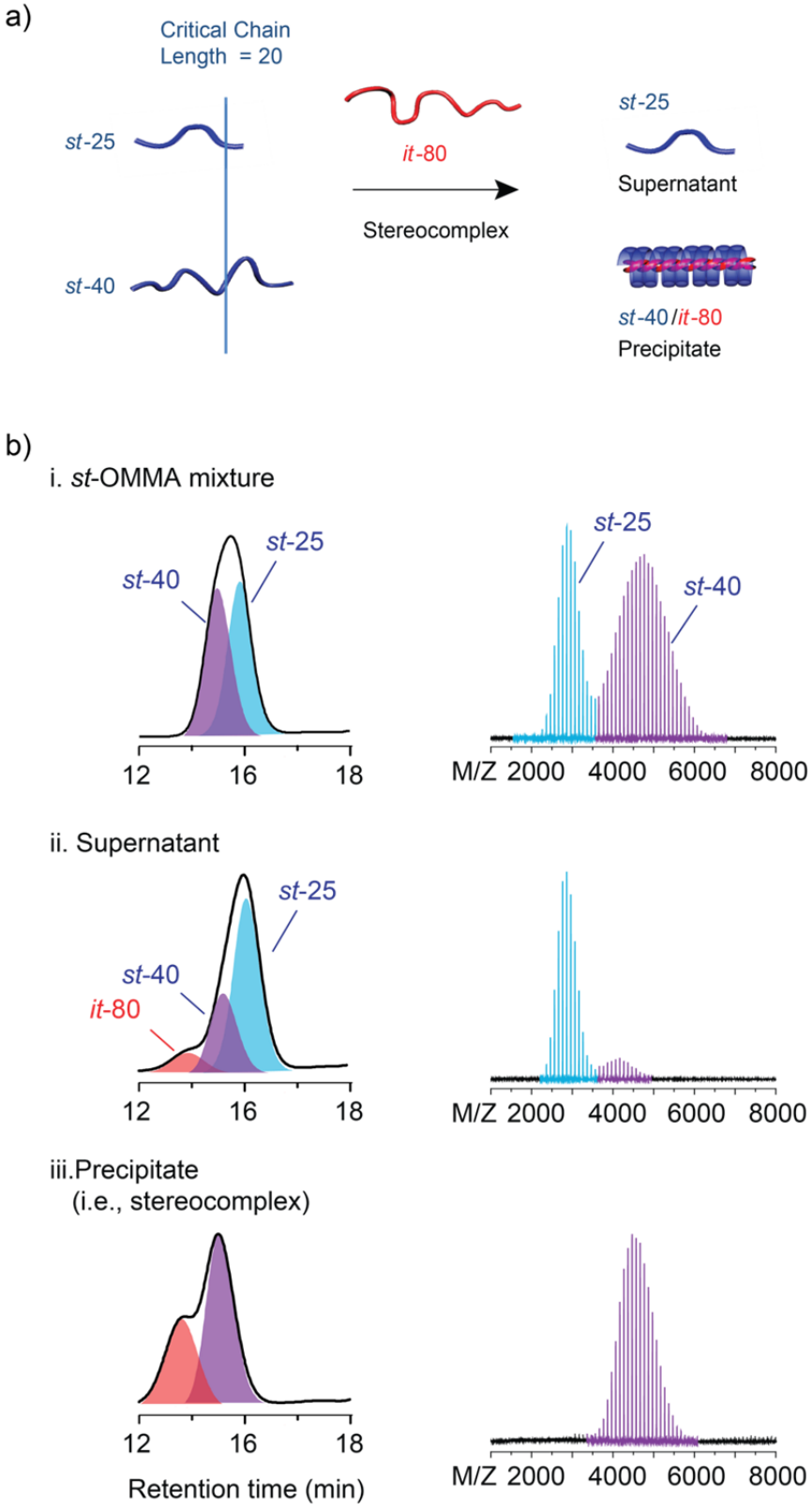

Figure S14. (a) Schematic illustration of molecular separation through stereocomplex formation (*it*-/*st*- molar ratio = 1:4). (b) GPC (deconvoluted; see **Figure S17K-M** for details) and MALDI-ToF MS of (i) *st*-25 and 40 mixture, (ii) the supernatant, and (iii) the precipitate of the reaction solution. **Note:** MS peaks due to *it*-80 could not be observed due to preferential ionization of the lower MW *st*-oligomers.[10]

***SI-16*. Molecular separation of *st*-40 and 60 through stereocomplex formation with *it*-80**

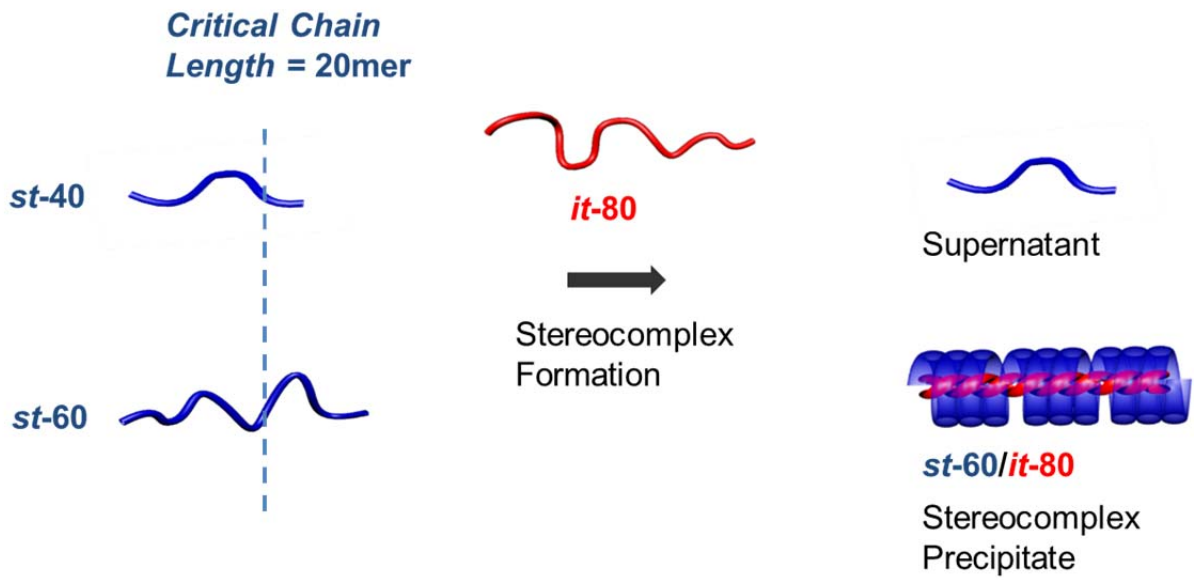

Figure S15a. Schematic illustration of molecular separation of *st*-40 and 60 through stereocomplex formation with *it*-80 (*it*-/*st*- molar ratio = 1:4).

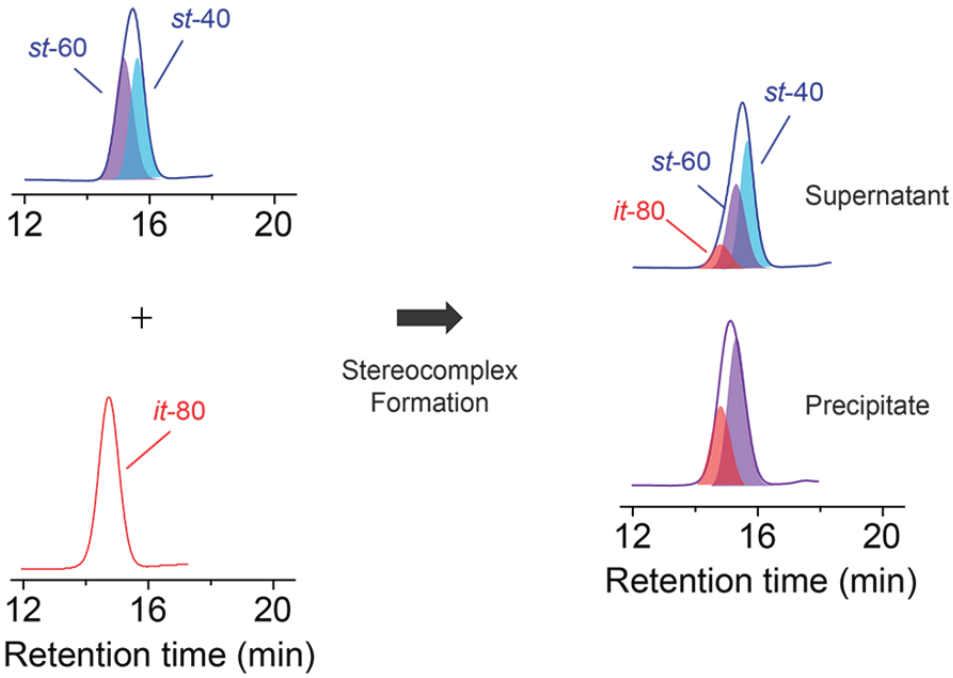

Figure S15b. GPC traces of *st*-40 and 60 mixture, *it*-80, the supernatant, and the precipitate of the reaction solution (*it*-/*st*- molar ratio = 1:4).

***SI-17*. Molecular separation of *it*-40 and 60 through stereocomplex formation with *st*-80**

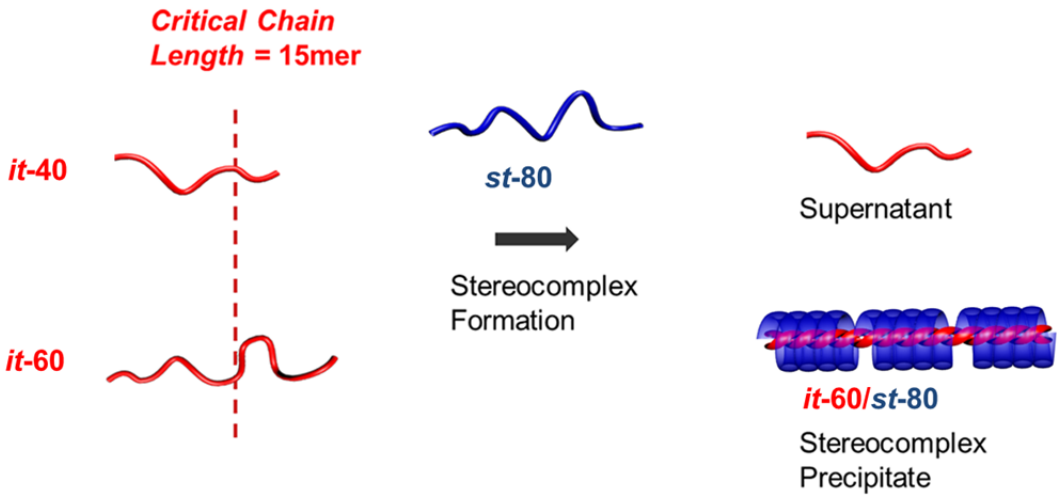

Figure S16a. Schematic illustration of molecular separation of *it*-40 and 60 through stereocomplex formation with *st*-80 (*it*-/*st*- molar ratio = 1:1).

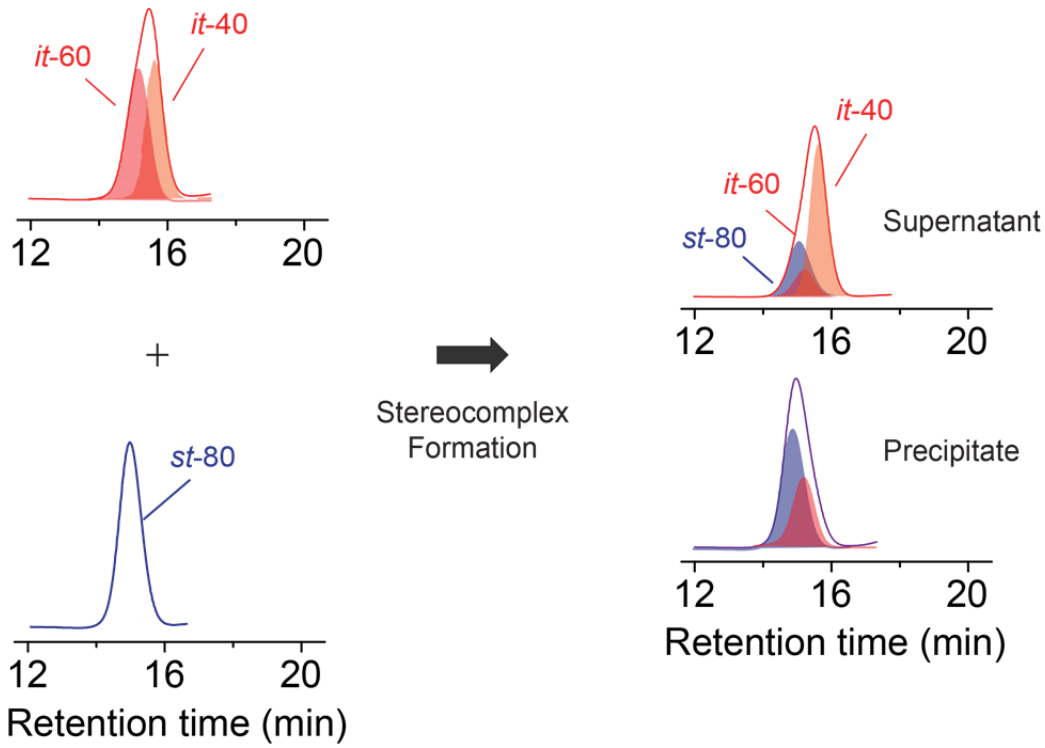

Figure S16b. GPC traces of *st*-40 and 60 mixture, *st*-80, the supernatant, and the precipitate of the reaction solution (*it*-/*st*- molar ratio = 1:1).

SI-18. **Other characterization data**

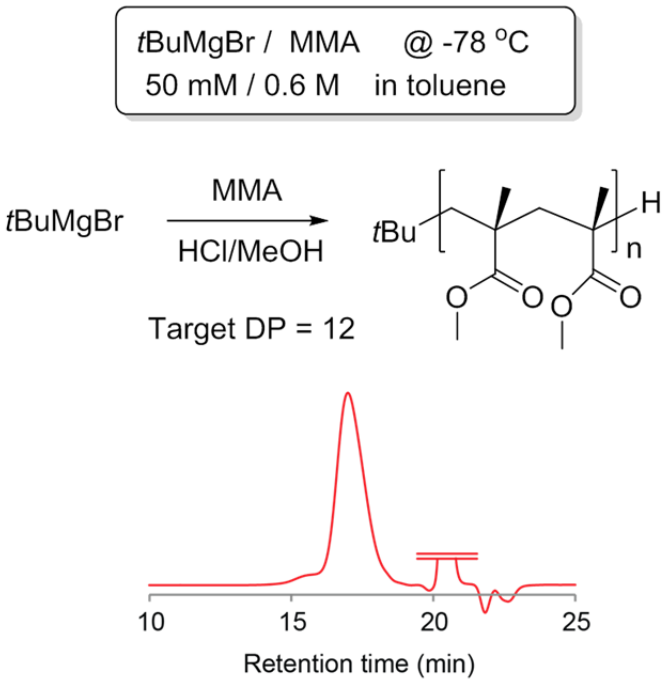

Code	Time (hr)	Conv. (%)	Yield (g)	M_n^{GPC} (*k*Da)	PDI
JMR012	30	99%+	3.5 (83%+)	2.7	1.2

Figure S17a. Representative GPC trace and data of the crude *it*-OMMA synthesized.

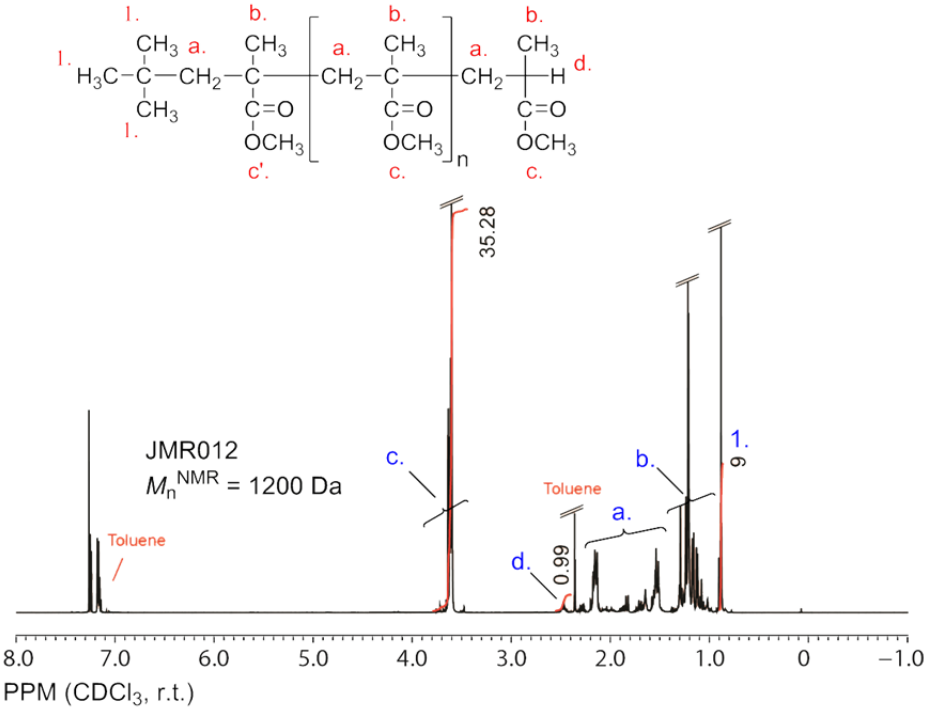

Figure S17b. Representative ^{1}H NMR spectrum of the crude *it*-OMMA synthesized.

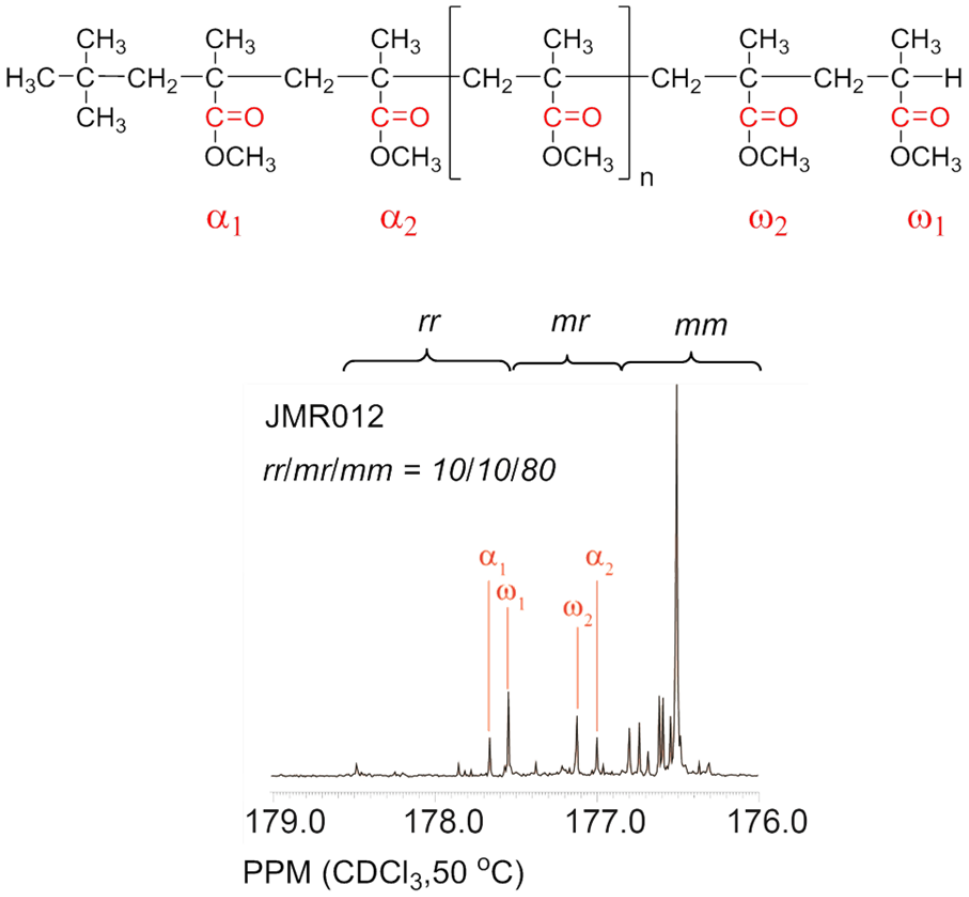

Figure S17c. Representative partial ^{13}C NMR spectrum of the crude *it*-OMMA synthesized (the C=O group resonance was used to determine the tacticity).

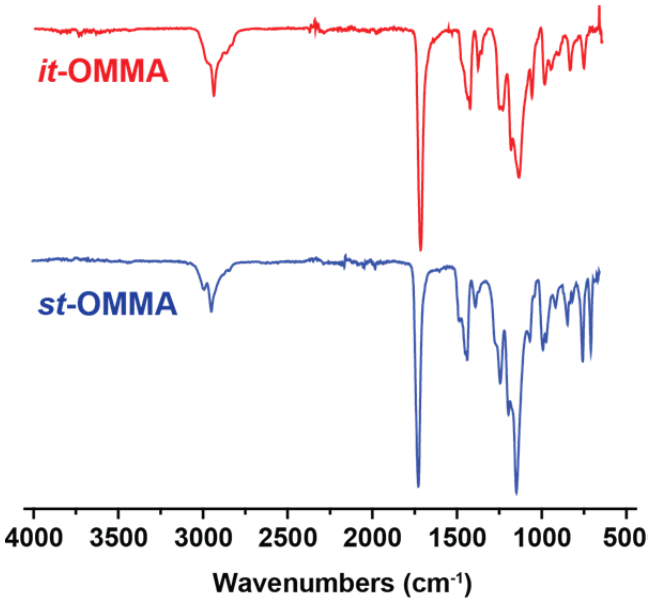

Figure S17d. Representative FT-IR spectra of the crude *it*-OMMA ($M_{n,NMR}$ = 1.2 *k*Da, $Đ_{GPC}$ = 1.2) and *st*-OMMA ($M_{n,NMR}$ = 1.9 *k*Da, $Đ_{GPC}$ = 1.2) synthesized.

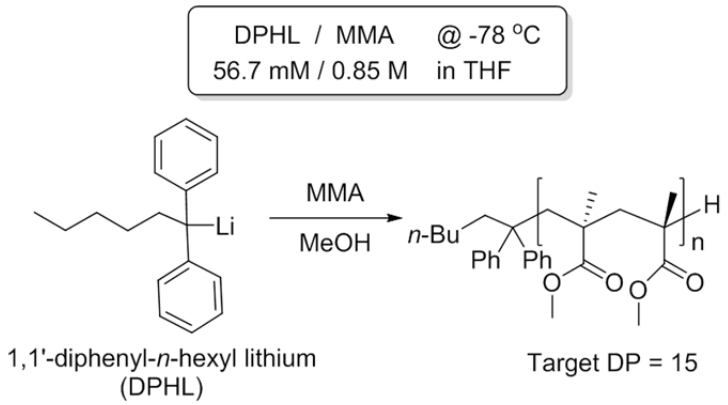

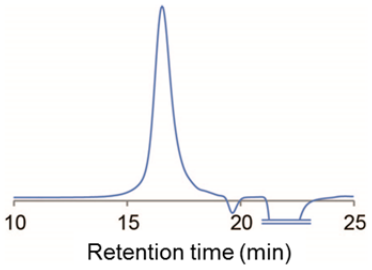

Code	Time (mins)	Conv. (%)	Yield (g)	M_n^{GPC} (kDa)	PDI
JMR007	70	99%+	5.0 (95%)	2.4	1.2

Figure S17e. Representative GPC trace and data of the crude *st*-OMMA synthesized.

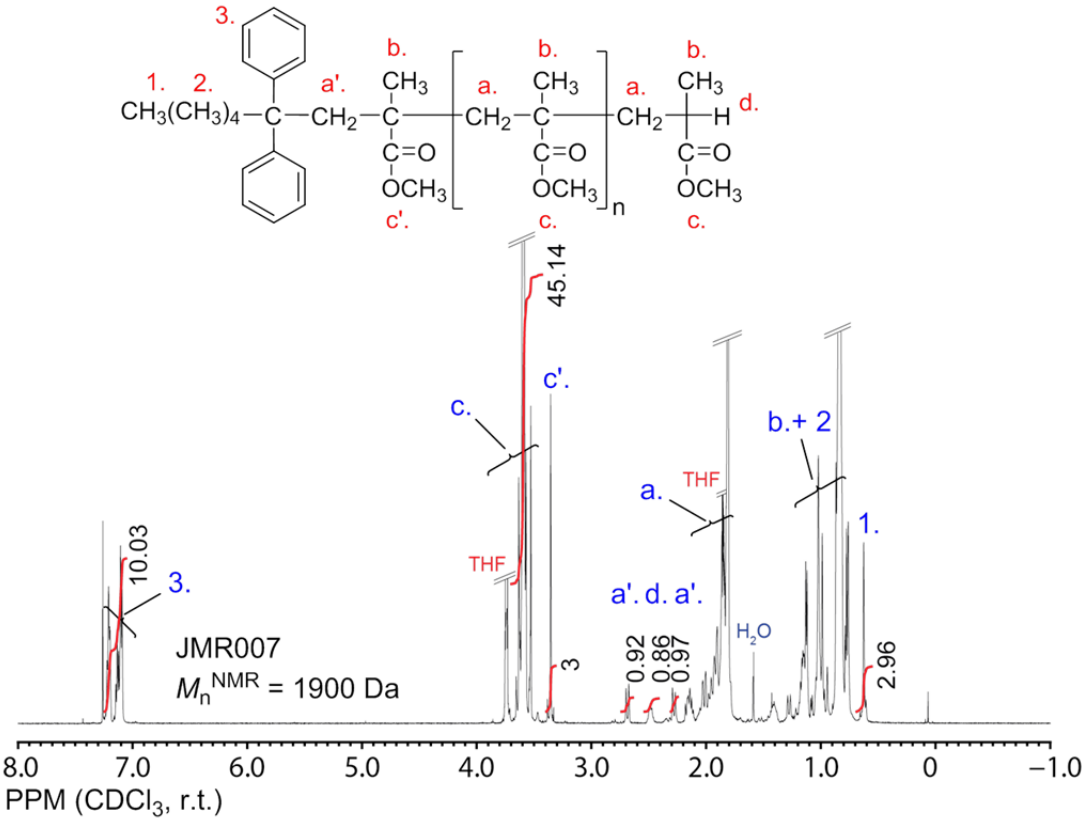

Figure S17f. Representative ^{1}H NMR spectrum of the crude *st*-OMMA synthesized.

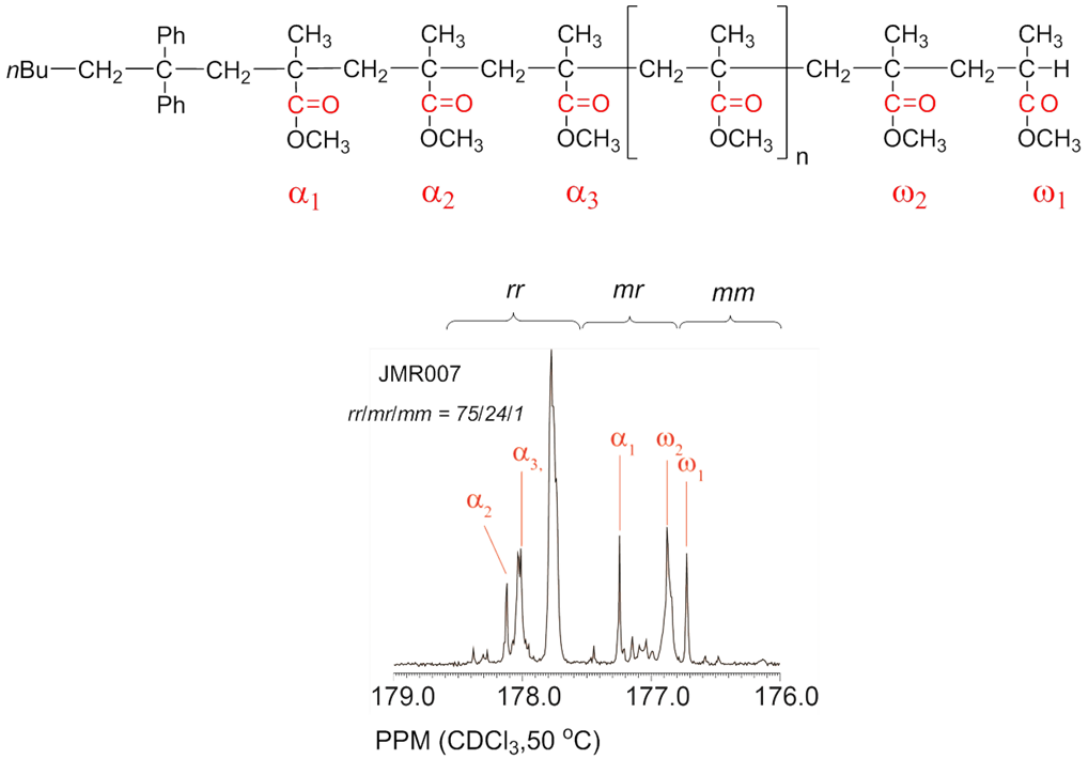

Figure S17g. Representative partial ^{13}C NMR spectrum of the crude *st*-OMMA synthesized (the C=O group resonance was used to determine the tacticity).

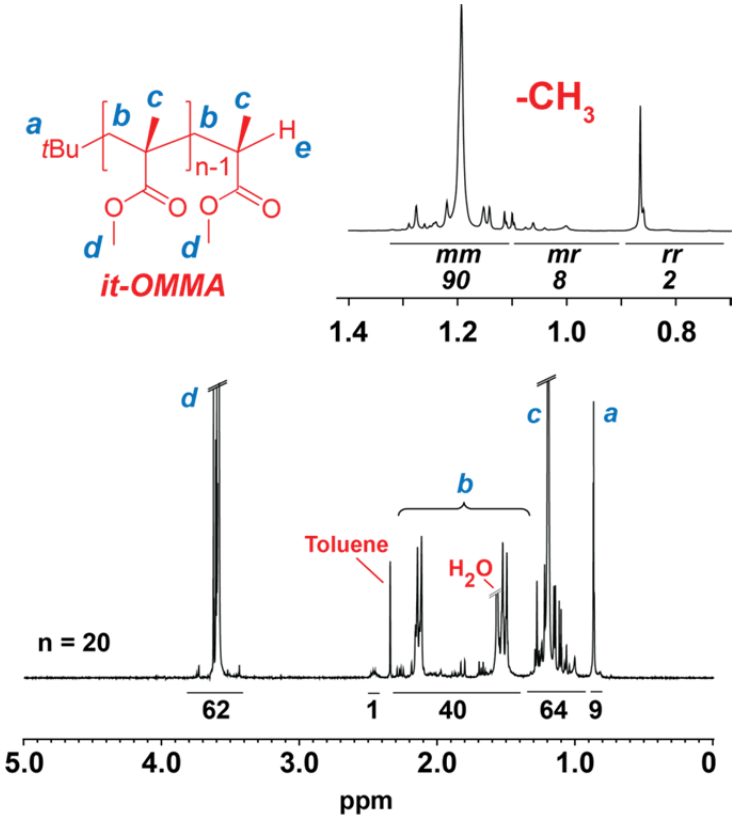

Figure S17h. ^{1}H NMR spectrum of *it*-20 isolated through the gradient flash chromatography *Inset*: tacticity determination based on integration of proton resonance of backbone -CH_3 units.

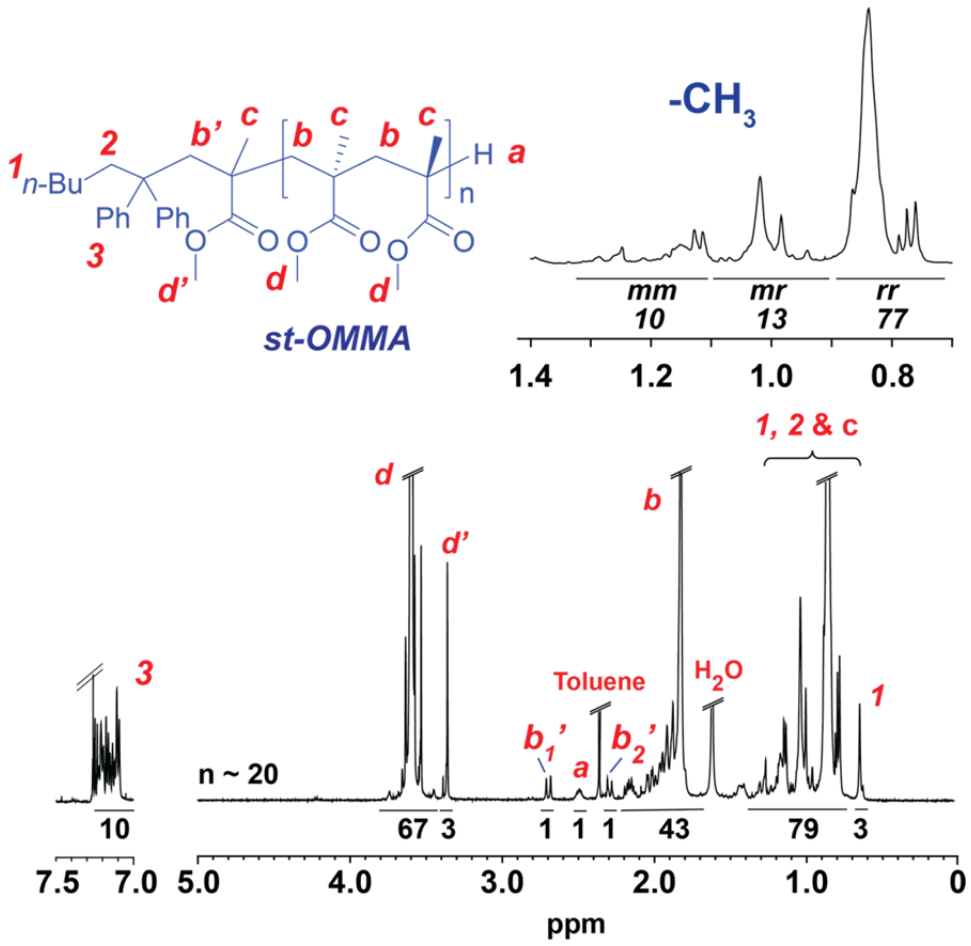

Figure S17I. ^{1}H NMR spectrum of *st*-20 isolated through the gradient flash chromatography *Inset*: tacticity determination based on integration of proton resonance of backbone -CH_3 units.

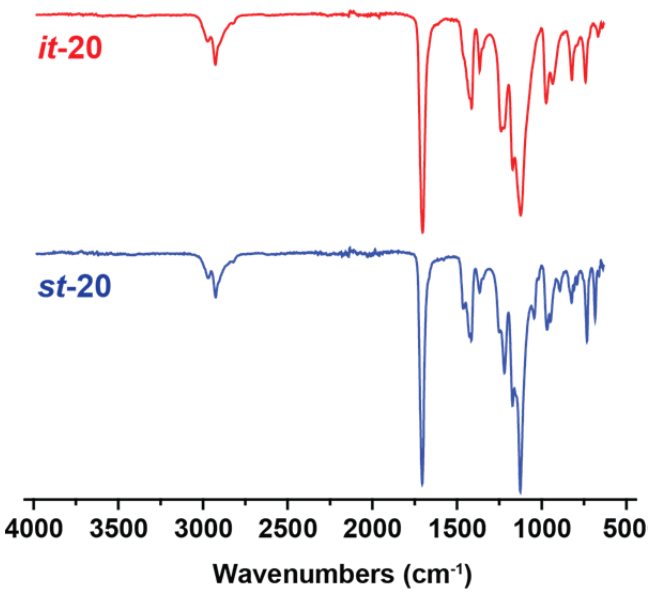

Figure S17J. FT-IR spectra of *st*-/*it*-20 isolated through the gradient flash chromatography.

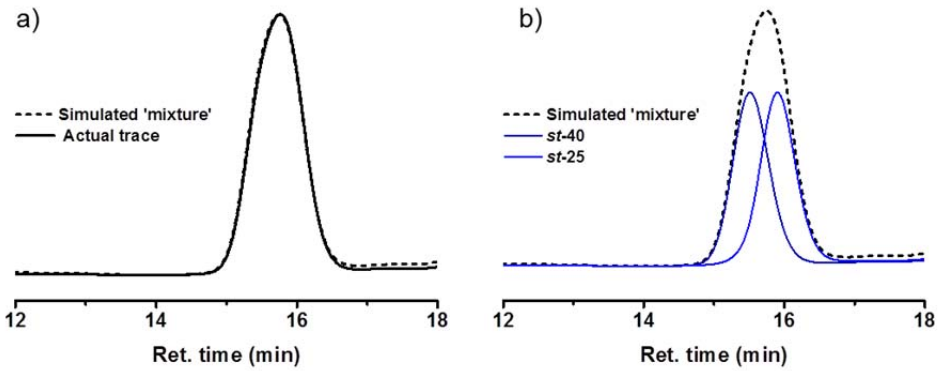

Figure S17K. Representative GPC deconvolution of *st*-OMMA mixture (*st*-25 and *st*-40), a) the comparison of the actual dRI trace and the simulated trace, and b) the simulated dRI trace based on the GPC traces of *st*-25 and *st*-40.

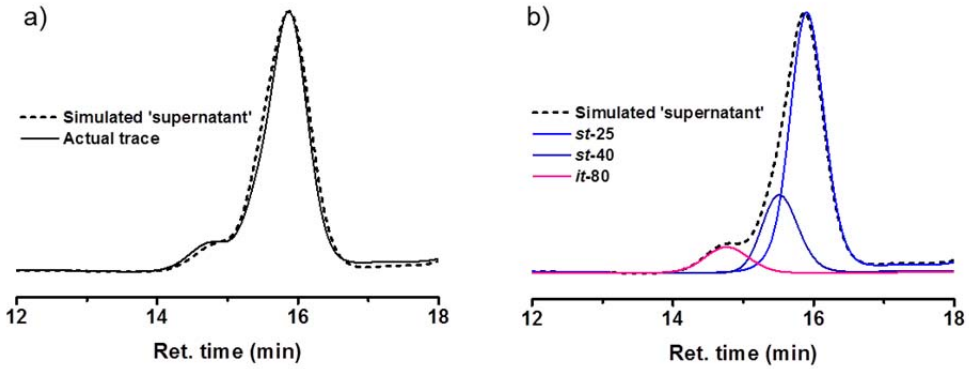

Figure S17L. Representative GPC deconvolution of the supernatant of the MW separation experiment (*st*-25, *st*-40, and *it*-80), a) the comparison of the actual dRI trace and the simulated trace, and b) the simulated dRI trace based on the GPC traces of *st*-25, *st*-40, and *it*-80.

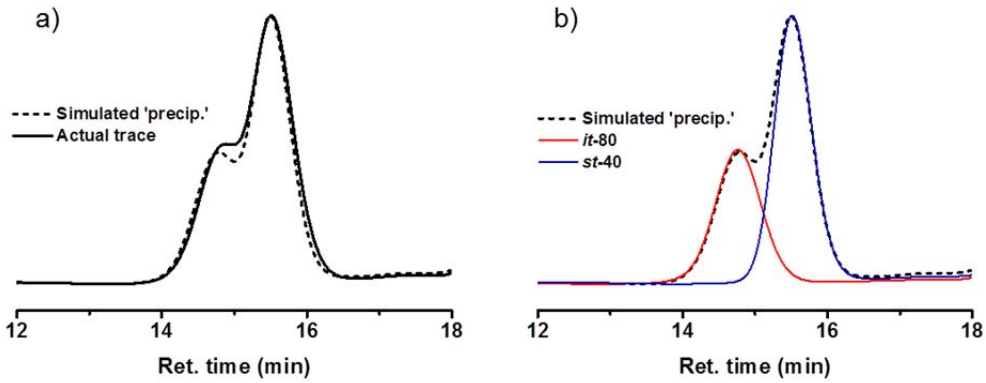

Figure S17M. Representative GPC deconvolution of the precipitate of the MW separation experiment (*st*-25, *st*-40, and *it*-80), a) the comparison of the actual dRI trace and the simulated trace, and b) the simulated dRI trace based on the GPC traces of *st*-40 and *it*-80 (2 : 1 weight ratio).

Reference

(1) Ren, J. M.; Ishitake, K.; Satoh, K.; Blencowe, A.; Fu, Q.; Wong, E. H. H.; Kamigaito, M.; Qiao, G. G., *Macromolecules* **2016**, *49*, 788.

(2) Sato, M.; Kato, T.; Ohishi, T.; Ishige, R.; Ohta, N.; White, K. L.; Hirai, T.; Takahara, A., *Macromolecules* **2016**, *49*, 2071.

(3) Li, Y.; Beck, R.; Huang, T.; Choi, M. C.; Divinagracia, M. *J. Appl. Crystallogr.* **2008**, *41*, 1134.

(4) Hatada, K.; Ute, K.; Tanaka, K.; Kitayama, T.; Okamoto, Y. *Polym. J.* **1985**, *17*, 977

(5) Ren, J. M.; Satoh, K.; Goh, T. K.; Blencowe, A.; Nagai, K.; Ishitake, K.; Christofferson, A. J.; Yiapanis, G.; Yarovsky, I.; Kamigaito, M.et al. *Angew. Chem., Int. Ed.* **2014**, *53*, 459.

(6) Cao, Z.-K.; Okamoto, Y.; Hatada, K. *Kobunshi Ronbunshu* **1986**, *43*, 857.

(7) Lawrence, J.; Lee, S.-H.; Abdilla, A.; Nothling, M. D.; Ren, J. M.; Knight, A. S.; Fleischmann, C.; Li, Y.; Abrams, A. S.; Schmidt, B. V. K. J.et al. *J. Am. Chem. Soc.* **2016**, *138*, 6306.

(8) Goh, T. K.; Tan, J. F.; Guntari, S. N.; Satoh, K.; Blencowe, A.; Kamigaito, M.; Qiao, G. G. *Angew. Chem., Int. Ed.* **2009**, *48*, 8707.

(9) a) Schomaker, E.; Challa, G., *Macromolecules* **1988**, *21*, 2195; b) Schomaker, E.; Hoppen, H.; Challa, G., *Macromolecules* **1988**, *21*, 2203.

(10) Montaudo, G.; Montaudo, M. S.; Puglisi, C.; Samperi, F., *Rapid Commun. Mass Spectrom.* **1995**, *9*, 453.

.